Published OnlineFirst April 9, 2019; DOI: 10.1158/1541-7786.MCR-18-1045

CANCER "-OMICS"

Molecular Cancer Research

Characterization of HCC Mouse Models: Towards an Etiology-Oriented Subtyping Approach

Juliane Friemel[1], Lukas Frick[1,2], Kristian Unger[3], Michele Egger[1], Rossella Parrotta[1], Yannick T. Böge[1], Arlind Adili[1], Michael Karin[4], Tom Luedde[5], Mathias Heikenwalder[6], and Achim Weber[1]

Abstract

Murine liver tumors often fail to recapitulate the complexity of human hepatocellular carcinoma (HCC), which might explain the difficulty to translate preclinical mouse studies into clinical science. The aim of this study was to evaluate a subtyping approach for murine liver cancer models with regard to etiology-defined categories of human HCC, comparing genomic changes, histomorphology, and IHC profiles. Sequencing and analysis of gene copy-number changes [by comparative genomic hybridization (CGH)] in comparison with etiology-dependent subsets of HCC patients of The Cancer Genome Atlas (TCGA) database were conducted using specimens (75 tumors) of five different HCC mouse models: diethylnitrosamine (DEN) treated wild-type C57BL/6 mice, c-Myc and AlbLTαβ transgenic mice as well as TAK1^{LPC-KO} and Mcl-1$^{\Delta hep}$ mice. Digital microscopy was used for the assessment of morphology and IHC of liver cell markers (A6-CK7/19, glutamine synthetase) in mouse and $n = 61$ human liver tumors. Tumor CGH profiles of DEN-treated mice and c-Myc transgenic mice matched alcohol-induced HCC, including morphologic findings (abundant inclusion bodies, fatty change) in the DEN model. Tumors from AlbLTαβ transgenic mice and TAK1^{LPC-KO} models revealed the highest overlap with NASH-HCC CGH profiles. Concordant morphology (steatosis, lymphocyte infiltration, intratumor heterogeneity) was found in AlbLTαβ murine livers. CGH profiles from the Mcl-1$^{\Delta hep}$ model displayed similarities with hepatitis-induced HCC and characteristic human-like phenotypes (fatty change, intertumor and intratumor heterogeneity).

Implications: Our findings demonstrate that stratifying preclinical mouse models along etiology-oriented genotypes and human-like phenotypes is feasible. This closer resemblance of preclinical models is expected to better recapitulate HCC subgroups and thus increase their informative value.

Introduction

Hepatocellular carcinoma (HCC) is the most common primary liver cancer and has become the third leading cause of cancer-related death worldwide (1, 2). The main risk factors for liver carcinogenesis are chronic liver diseases, such as viral hepatitis, alcoholic, or nonalcoholic steatohepatitis (ASH/NASH), exposure to aflatoxin or genetic disposition (e.g., α1-antitrypsin deficiency; ref. 3). Dietary-induced liver cancer is an emerging problem in developed as well as in developing countries (4, 5).

Strategies to improve the still poor survival of HCC patients rely on preclinical mouse models, such as cell line–derived models in immunocompromised mice (allografts and xenografts), genetically engineered mouse models (GEMM) and environmentally induced models. So far, the translational value of mouse models with respect to patient benefit has frequently fallen behind expectations. Besides the need for discovering new anti-HCC targets and compounds and testing them *in vivo*, it is of utmost importance to improve analyses and subtyping for preclinical mouse model research. First, distinct models may recapitulate only individual features of human HCC. Second, reporting of morphology, IHC profiles, genetic landscapes, sequencing of the key tumor suppressors/oncogenes, and growth monitoring of murine tumors is poorly standardized in mouse research (6). An important challenge in the comprehensive characterization of murine models is already to identify truly malignant lesions. Different criteria are used, such as atypia, increased proliferation, expansive growth, necrosis, or extracapsular invasion (7–9). Markers such as glutamine synthetase and collagen IV may serve as supplemental indicators for tumor diagnosis (10–12). Mutational profiles of murine liver tumors, with frequent *CTNNB1* mutations and rare or absent *TP53* alterations, were characterized in earlier studies (13–15).

Approaches to improve mouse model characterization and subtyping include (i) systematic assessment of human-like

[1]Department of Pathology and Molecular Pathology, University and University Hospital Zurich, Zurich, Switzerland. [2]Swiss Hepato-Pancreato-Biliary Center, Department of Digestive and Transplant Surgery, University Hospital of Zurich, Zurich, Switzerland. [3]Helmholtz Zentrum München Research Center for Environmental Health (GmbH), Research Unit Radiation Cytogenetics. [4]Department of Pathology, University of California, San Diego, California. [5]Department of Medicine III, University Hospital RWTH Aachen, Aachen, Germany. [6]Division Chronic Inflammation and Cancer, German Cancer Research Center, Heidelberg, Germany.

Note: Supplementary data for this article are available at Molecular Cancer Research Online (http://mcr.aacrjournals.org/).

J. Friemel and L. Frick share first authorship and A. Weber and M. Heikenwalder share last authorship of this article.

Corresponding Authors: Achim Weber, University of Zurich, Schmelzbergstr. 12, Zurich 8091, Switzerland. Phone: 41-44-2552781; Fax: 44-2554416; E-mail: achim.weber@usz.ch; and Mathias Heikenwalder, Division Chronic Inflammation and Cancer, German Cancer Research Center, Heidelberg, Germany. Phone: 49-6221423891; E-mail: m.heikenwaelder@dkfz.de

Mol Cancer Res 2019;17:1493–502

doi: 10.1158/1541-7786.MCR-18-1045

Published OnlineFirst April 9, 2019; DOI: 10.1158/1541-7786.MCR-18-1045

Table 1. Genetic background and phenotypic presentation of mouse models

Model	Genetic background	Mode	Phenotype of tumors as originally documented	Phenotype of surrounding liver tissue as originally documented	Average age at tumor development	Reference
DEN wt	C57BL/6/129	Chemically induced DNA damage (DEN)	Incidence lower in female animals and younger animals, typical liver histology	Liver injury and cell death, proliferative response	8–10 months	Maeda et al. 2005
c-Myc	C57BL/6J-CBA/J	Transgenic model with oncogene overexpression leading to genomic instability	Solid or trabecular histologic type, atypia, polymorphism, hemorrhagic necrosis	Transition of mild to severe dysplasia in hepatocytes, benign lesion ("adenoma")	12–15 months	Thorgeirsson et al. 1996
$TAK1^{LPC-KO}$	C57BL/6-SV129Ola	Knockout model with TAK1 deficiency, enhanced liver cell proliferation	Ductopenia, fibrosis, liver cell apoptosis, necrosis, hyperproliferation	Expansive growth, high cellularity, anisokaryosis of hepatocytes	4 months	Bettermann et al. 2010 Vucur et al. 2013
AlbLTαβ	CL57BL/6	Transgenic model with overexpression of cytokines, indirectly leading to cell damage	Multicentric nodules in tg 1223 mice, high proliferation, loss of collagen IV network	Infiltration of lymphocytes and macrophages, increased proliferation (A6+ cells)	12 months	Haybaeck et al. 2009
$Mcl\text{-}1^{\Delta hep}$	C57BL/6	Deficiency of antiapoptotic Mcl-1 with enhanced liver cell apoptosis and hyperproliferation	Altered liver architecture, cellular atypia, loss of collagen IV, immunoreactivity for glutamine synthetase	Apoptosis, pericellular fibrosis, enhanced proliferation	12 months	Vick et al. 2009 Weber et al. 2010 Boege et al. 2017

phenotypes including morphology, IHC profiles, and intratumor heterogeneity; (ii) evaluation of etiology-dependent models; and (iii) if possible, assignment to a clinically stratified patient subgroup. The murine models analyzed in this study comprise four GEMMs and one environmentally induced model, all with spontaneous, orthotopic tumor growth. Different genetic backgrounds were included, covering essential cancerogenesis pathways (8, 10, 11, 16–18): oncogene overexpression (c-Myc), chronic inflammation ($TAK1^{LPC-KO}$ and AlbLTαβ), and liver cell loss with compensatory proliferation ($Mcl\text{-}1^{\Delta hep}$). The "classical" and widely used DEN model was included, because it is generally considered to mimic toxin-induced cancerogenesis (7).

The aim of our study was to subtype HCC mouse models with different cancerogenesis backgrounds, to increase the translational value of rodent models. On the basis of comparative genomic hybridization (CGH) analysis, we propose a novel strategy to quantify the similarity of murine and human tumors. The starting criterion was the percentage of genomic overlap in the synteny analysis of CGH data of murine tumors compared with HCC patients of The Cancer Genome Atlas (TCGA) database. Furthermore, we categorized histomorphologic features and IHC profiles to show different qualities and levels of overlap. Each set of murine tumors (DEN treatment, c-Myc induced, $TAK1^{LPC-KO}$ knockout, AlbLTαβ transgenic mice, and $Mcl\text{-}1^{\Delta hep}$ knockout) was compared with three clinically defined subsets of human HCC (alcohol, chronic viral hepatitis, NASH/cryptogenic) and molecular subclasses G1–6, in order to identify which rodent model recapitulates HCC carcinogenesis in specific etiologic backgrounds. Our approach might help future guidelines to stratify and compare preclinical mouse models—finally helping to increase the success rate in clinical trials.

Materials and Methods

Murine tissues

Formalin-fixed, paraffin-embedded (FFPE) mouse liver tissues retrieved from previous studies as listed in Table 1 were used (7, 10, 11, 16, 17). Original experiments with mice had been conducted in concordance with local guidelines (approval: "Tierversuchsgenehmigung vom Kantonalen Veterinäramt Zürich 63/2011"). Five mouse models were used: In the DEN models, tumors were chemically induced in wild-type (C57BL/6 strain) mice (7). The c-Myc model is a transgenic model targeting the c-Myc proto-oncogene (16). In the $TAK1^{LPC-KO}$ model, specific depletion of $TAK1^{LPC-KO}$ in liver parenchymal cells leads to deregulated TNF signaling as well as defective AMPK activation resulting in chronic mTORC1 activation (19). Liver cells undergo uncontrolled proliferation and necroptosis/apoptosis leading to early, accelerated liver cancer formation in mice (17, 20). The transgenic AlbLTαβ/tg+ model reflects inflammation-induced carcinogenesis with aberrant expression of the cytokine lymphotoxin (10). The $Mcl\text{-}1^{\Delta hep}$ model mimics chronic liver cell damage through hepatocyte-specific depletion of the antiapoptotic protein myeloid cell leukemia 1, which leads to continual hepatocyte apoptosis, increased cell turnover, compensatory proliferation, and spontaneous tumor formation (8, 11).

Mutation analysis and CGH

For mutation analysis and CGH ($n = 75$), DNA was extracted from FFPE tissues (Kit, GE-healthcare). PCR was performed with following the manufacturer's protocols (AmpliTaq Gold, Applied Biosystems), conducting 40 cycles (*TP53* exons 5–8, *CTNNB1*) or 35 cycles (*BRAF*, *HRAS*). Primers were used as previously described: *CTNNB1* exon 2 (21), *TP53* exons 5–8 (22), *HRAS*, and *BRAF* (23). Annealing temperatures were 56°C (*TP53* exons 6 and 8, *BRAF*, *HRAS*) or 60°C (*TP53* exons 5 and 7). PCR amplification and sequencing of the mTERT core promoter fragment (24, 25) was performed on a subset of tumors ($n = 31$ tumor samples) and 10 unaffected tissues. We used (−279 to +14 coverage) two primer pairs, forward 1/2: TTA CTC CAA CAC ATC CAG CAA and CCT TCC GCT ACA ACG CTT; reverse 1/2: AAA GAT GAG GCT GGG AAC G and GAG CGC GGG TCA TTG TG, at 58°C annealing temperature. Sequencing was performed using a commercial service (Microsynth) with dropouts (1%–10%) due to poor DNA quality. Mutation analysis was performed using BioEdit freeware, GRCm38/mm9 served as the reference genome. For

Published OnlineFirst April 9, 2019; DOI: 10.1158/1541-7786.MCR-18-1045

CGH analysis, commercially available kits (Oligonucleotide Array-Based CGH for Genomic DNA Analysis, Agilent) were used (26), and CGH results were matched with results from the TCGA cohort (TCGA-LIHC; http://cancergenome.nih.gov/. Synteny analysis of CGH data was performed according to the theory of eutherian chromosome evolution (27). Contingency tables were constructed with etiology-dependent HCC subsets such as alcohol-related, hepatitis B/C-induced, or NASH-induced/cryptogenic HCC. Cryptogenic HCC were used for the analysis because these tumors are likely caused by burned out NASH even in the absence of cirrhosis (28–30). Fisher's exact test was used for statistical analysis, adjusted for multiple testing (Benjamini–Hochberg correction). A significance level of 5% was set to detect significant correlations between human and mouse chromosomal losses and gains controlling for the alpha error. The classification of HCC proposed by Boyault and colleagues (31) into the subgroups G1–6 was applied to TCGA cohort. The data set E-TABM-36 was retrieved from ArrayExpress (ebi.ac.uk/arrayexpress) and class labels were extracted from Fig. 1 of Boyault and colleagues. An additional data set, GSE62232, was retrieved from GEO (ncbi.nlm.nih.gov/geo), and class labels were kindly provided by the authors. A list of top overexpressed genes per subgroup was produced by comparing patients in each subgroup with patients in all other subgroups. These lists were then used to classify patients from the TCGA cohort into the six subgroups using the Nearest Template Prediction algorithm (32).

Morphology and IHC

A systematic review of the documented murine models was performed (10, 11, 16, 17). For virtual microscopy, we digitalized slides of murine liver lesions with available IHC results ($n = 149$) using a NanoZoomer C9600 Virtual Slide Light microscope scanner by Hamamatsu using NDP, View Software, version 1.2.36.

Murine liver lesions were classified as tumors based on morphologic criteria reported by Thoolen and colleagues (9) and five markers of liver pathology (Supplementary Fig. S1). Briefly, overgrowth compressing the normal tissue and/or distortion of the lobular architecture was considered as the main criteria for tumors in contrast to dysplastic nodules. Collagen IV loss or broadening of trabecular structures was regarded as neoplastic growth. Cytological features considered as indicators for malignancy were cell polymorphism, atypia, increased nucleus–cytoplasm ratio, inclusion bodies, or basophilia. Sizes of cells and nuclei were measured using digitalized histologic pictures and dichotomized by the median. The tumor grading was based on a combination of nuclei sizes (<10 μm = 1, 10–15 μm = 2, 15–20 μm = 3), presence of nucleoli and cell–plasma ratio (decreased/normal). Proliferation in tumors was assessed as a 4-point scale (none, few, many, and abundant).

IHC on mouse tissues (glutamine synthetase, A6, GP73, collagen IV, Ki-67) was performed as described (10, 17). For human liver tissues, stainings of glutamine synthetase, CK7 and CK19, were conducted and scored as reported (33). Positivity for a marker was defined as follows: A6 and CK7/19: >10% of tumor cells, glutamine synthetase: diffuse strong staining of >50% cells, GP73: weak or strong positivity. For statistical analysis of morphologic features, IHC and mutational profiles, SPSS software was used (IBM SPSS, Version 21).

Human tissues samples

Human liver tissues were retrieved from the archives and biobank of the Department of Pathology and Molecular Pathology, University Hospital Zurich. Tissue microarrays (TMA) with duplicates of a total of 61 HCC patients and 60 matched controls were used for IHC analysis as described (34). Follow-up data for all patients were available. The study was reviewed and approved by the Cantonal Ethics Committee of Zurich, Switzerland, according to guidelines (KEK-ZH-Nr. 2013-0382).

Results

Tumor characteristics of different liver cancer mouse models

First, we aimed to perform a systematic histopathologic characterization comparing murine livers of all models (Table 2). Analysis of a total 49 mouse livers with an average of ~3 tumors per mouse (mean 3.04 ± 0.81) revealed several differences among the five mouse models. Smaller, rather monomorphic tumors and numerous dysplastic lesions were found in the DEN-treated and TAK1$^{LPC\text{-}KO}$ models, compared with larger, less-abundant tumors in the c-Myc, the Mcl-1$^{\Delta hep}$, and the AlbLTαβ models. In the Mcl-1$^{\Delta hep}$ model, subnodules were observed, which were reminiscent of those observable in human HCC (33). The size of cells and nuclei in individual tumors was higher in the TAK1$^{LPC\text{-}KO}$ and AlbLTαβ models compared with those in other models. High-grade tumors, defined by a combination of large nuclei, presence of nucleoli, and an increased nuclear/cytoplasmatic ratio were found in the TAK1$^{LPC\text{-}KO}$ and the AlbLTαβ models (67% and 83% of tumors, respectively). High proliferation was found in tumors of the Mcl-1$^{\Delta hep}$ model (21 tumors of total 38) and the c-Myc model (15 tumors of total 22).

Analysis of chromosomal gains and losses per mouse and tumor revealed patterns with predominant chromosomal gains (DEN, TAK1$^{LPC\text{-}KO}$) and patterns with predominant chromosomal losses (AlbLTαβ; Fig. 1A). In comparison with the unstratified TCGA reference HCC cohort, the percentage of combined aberrations (amplification and deletions) that overlapped between the murine tumors and human HCCs ranged from 56% in the TAK1$^{LPC\text{-}KO}$ model to 71% (mea$n = 61\%$) in the AlbLTαβ model (Table 2).

Targeted mutational analysis of commonly affected genes (*TP53*, *HRAS*, *NRAS*, *CTNNB1*, and *TERT*) showed that murine liver tumors across all mouse models were *TP53* wild-type (Fig. 1B). Thirty-three percent of analyzed DEN-induced tumors showed *BRAF* mutations, lower than previously reported (35). *CTNNB1* were found in the c-Myc model (10%) and in four liver tumors (21%) of the same animal within the Mcl-1$^{\Delta hep}$ group. At low frequency (max. 11%), *HRAS* mutations (DEN, Mcl-1$^{\Delta hep}$, and c-Myc models) were detected. *TERT* promoter mutations of the transcription factor binding sites were analyzed in a subset of murine tumor samples ($n = 31$) and were not detected.

A subtype-specific approach based on CGH synteny analysis

By comparing CGH profiles of distinct HCC patient subsets from the TCGA database with profiles of each mouse model, the mean overlap further increased by maximally 14% (Fig. 2A and B). Murine tumors of the DEN and c-Myc models shared genomic changes predominantly with alcohol-induced HCCs (63%–69%; $P < 0.01$) and the G5 molecular subclass. AlbLTαβ and TAK1$^{LPC\text{-}KO}$ most closely resembled NASH-HCC (57%–67%; $P < 0.01$) and the G3 molecular subclass. Mcl-1$^{\Delta hep}$ showed

Published OnlineFirst April 9, 2019; DOI: 10.1158/1541-7786.MCR-18-1045

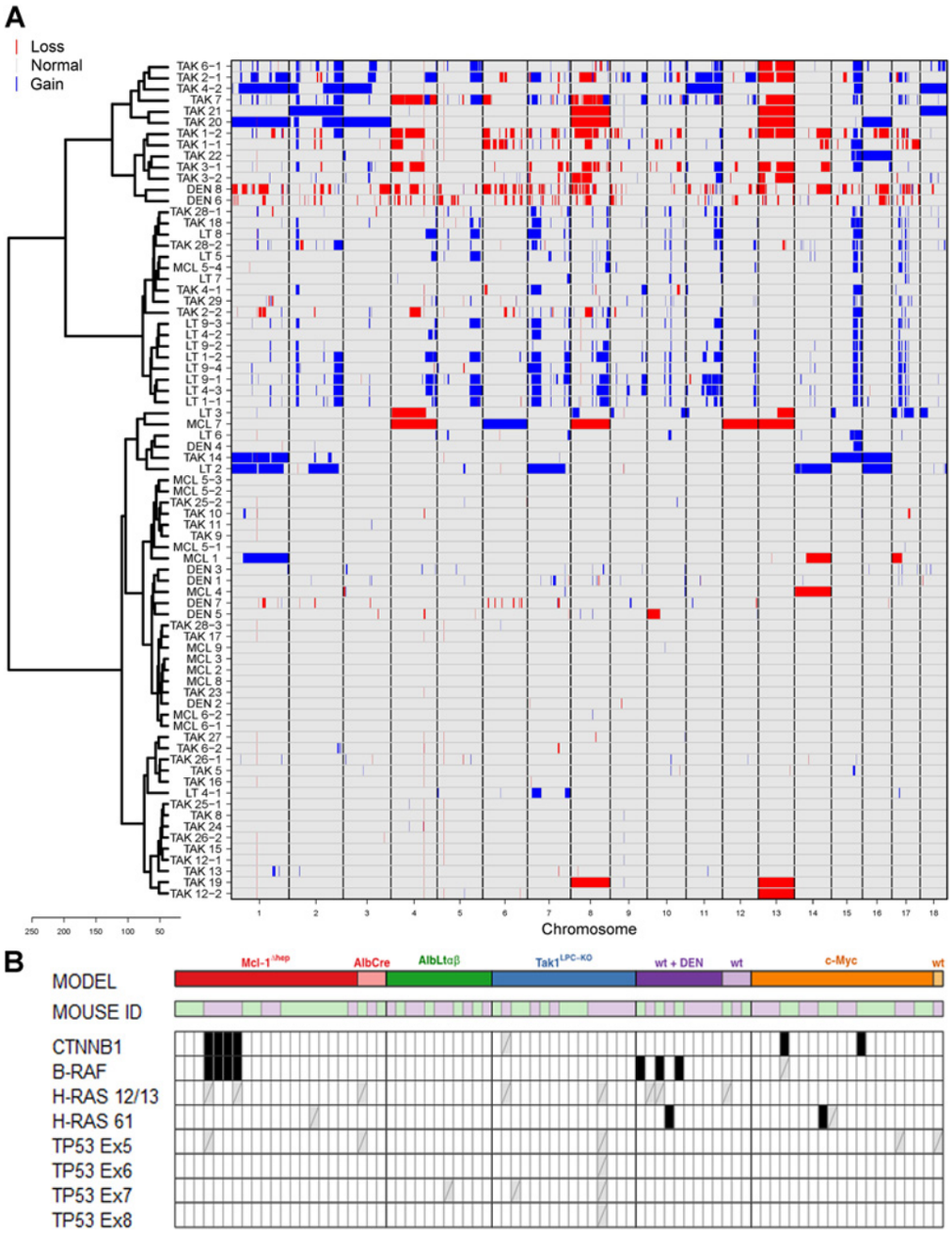

Figure 1

Genomic landscapes of murine liver tumors assessed by CGH and targeted sequencing. **A,** Unsupervised clustering of genomic aberrations of single mouse tumor samples. Left column displays type of mouse model with malignant liver tumor on C57Bl/6 background (DEN; DEN-induced, Myc; c-Myc, TAK; TAK1^{LPC-KO}, LT; AlbLTαβ and MCL; Mcl-1$^{\Delta hep}$). Color display shows chromosomal gains and losses per tumor (red: losses, blue: gains). Each line represents one sample (i.e., one mouse). Samples are clustered by genetic similarities. **B,** Sequencing results of targeted sequencing for most common gene altered in human HCC. Each square represents a sample (i.e., one murine tumor); squares are summarized by model including 1–3 control samples (wild-type). Black squares indicate mutations; crossed out gray squares indicate that the sample could not be sequenced due to quality reasons.

highest overlap with viral hepatitis-induced HCC (60%, $P < 0.01$) and the G3 molecular subclass.

We next tested whether morphologic findings support the CGH-based classification of murine tumors (Fig. 3A). In the DEN model, abundant cellular inclusions mimic Mallory–Denk bodies found in toxin-damaged liver cells. The presence of fatty change and clear cell cytology supports chronic nutritive-toxic liver cell damage. The c-Myc model was the second closest match for alcohol-induced cancer, based on CGH analysis. Histopathologic findings comprised clear cell features and pale inclusion bodies in

Published OnlineFirst April 9, 2019; DOI: 10.1158/1541-7786.MCR-18-1045

Table 2. Histomorphology and genetic characterization of murine liver tumors

Model	No. of tumors ($n = 149$)	No. of dysplastic lesions	Mean tumor size (mm)	Mutations[a] ($n = 73$)	CGH-based similarity to human HCC[b]	*P*-value CGH matches	Cell size	Proliferating tumors
DEN	19	146	3 ± 1.4	*BRAF* 3/9 *HRAS* 1/9	60.8 (losses) 65.8 (gains)	<0.01 0.636	Small	44%
c-Myc	22	10	6.9 ± 3.8	*CTNNB1* 2/19 *HRAS* 1/19	54.1 (losses) 57.5 (gains)	<0.01 <0.01	Medium	68%
TAK1^{LPC-KO}	37	118	2.9 ± 1.7	None (0/15)	47 (losses) 61.8 (gains)	<0.01 <0.01	Large	9%
AlbLTαβ	33	2	6.6 ± 3.3	None (0/11)	53.3 (losses) 72.3 (gains)	0.128 <0.01	Large	46%
Mcl-1$^{\Delta hep}$	38	79	5.6 ± 4.96	*BRAF* 4/19 *CTNNB1* 4/19	62.8 (losses) 63.7 (gains)	<0.01 0.113	Medium	55%

[a]Putations tested in subset, genes: *BRAF, HRAS, CTNNB1, TP53 (exons 5–8), TERT.*
[b]Percentages given by synteny analysis of murine tumors ($n = 75$) and unstratified human HCC cohort (TCGA).

combination with lymphocyte infiltration and distorted lobular architecture (Fig. 3B).

HCC of NASH/cryptogenic background matched closest with tumors from the TAK1^{LPC-KO} model and the AlbLTαβ model (CGH analysis). Histopathology showed steatosis, massive lymphocyte infiltration, and tumor necrosis in the AlbLTαβ model. NASH-typical morphologic findings were less frequent in the TAK1^{LPC-KO} model, possibly due to the early onset of carcinogenesis in this model. In contrast, a frequent finding was the mixed-cell phenotype, consisting of side-by-side eosinophilic and basophilic cells typically found in rodents and indicative of liver damage.

Mcl-1$^{\Delta hep}$ tumors most closely matched with virus-induced HCC than other etiologies based on CGH analysis (60%, $P < 0.004$), and the greatest overlap was seen with patients with hepatitis B ($P < 0.025$). Morphologically, tumors of the Mcl-1$^{\Delta hep}$ model showed apoptotic hepatocytes, highly proliferative tumors, tumor necrosis, steatosis, and moderate lymphocyte infiltration. Of note, fibrosis was rare in non-tumorous liver tissue throughout all models (Fig. 3C).

Intertumor and intratumor heterogeneity

Given that human HCC are mostly well-demarcated tumors with variable growth patterns and cytology, we next analyzed tumor growth including inter- and intratumor heterogeneity (32, 36). Intertumor heterogeneity refers to the diversity of tumors within each model, and is defined by the number of histology patterns per mouse cohort. Intratumor heterogeneity refers to the heterogeneity within each tumor, and is defined by histology patterns per individual tumor. As for the intertumor heterogeneity, we analyzed it on a morphological, IHC, and CGH level. Two of the models (DEN and TAK1^{LPC-KO}) scarcely showed any tumor heterogeneity, whereas three models (Mcl-1$^{\Delta hep}$, c-Myc, and AlbLTαβ) display tumor heterogeneity on a CGH level and histologically. In detail, a single major growth pattern and maximum two cytological features were found in the DEN model and the TAK1^{LPC-KO} model. In contrast, two (c-Myc model) or more than three growth patterns (Mcl-1$^{\Delta hep}$ and AlbLTαβ models) in combination with cytological features were observed (intertumor heterogeneity). Intratumor heterogeneity (>2 different growth patterns and/or cytological features within the same tumor) was present in ~50% of Mcl-1$^{\Delta hep}$ and AlbLTαβ tumors. In three of the models (DEN, Mcl-1$^{\Delta hep}$, AlbLTαβ), tumors were clearly demarcated compared with a diffuse intrahepatic growth in the other two models, i.e., c-Myc and TAK1^{LPC-KO} (Fig. 3D).

IHC profiles

Next, we were wondering whether IHC profiles in murine liver tumors mimicked the profiles of human HCC. Homogeneous IHC profiles were observed in the TAK1^{LPC-KO} model and the DEN-treated model. Tumors of the TAK1^{LPC-KO} model were nearly exclusively negative for A6 (biliary/progenitor phenotype) and glutamine synthetase (a marker of β-catenin activation) (36). Tumors of the DEN-treated mice were A6 positive in 85%. Heterogeneous, more human-like profiles were present in the c-Myc and Mcl-1$^{\Delta hep}$ models, including positivity for glutamine synthetase and/or A6. The closest resemblance to the HCC cohort IHC profile was found in the AlbLTαβ model (Fig. 4A and B).

In summary, murine tumors segregate into mainly biliary/progenitor-like phenotypes (DEN-treated, Mcl-1$^{\Delta hep}$), β-catenin-activated phenotype (c-Myc), and mixed (AlbLTαβ). Table 3 shows a summary of IHC, genetic and morphologic subtyping results.

Discussion

The challenge for future liver cancer models is to account for heterogeneity of disease, etiology-dependent pathogenesis, and therapeutic targets. Our approach suggests that these aspects should be considered to improve the clinical relevance and translational value of preclinical cancer research models.

Taking advantage of CGH, we were able to discriminate between preclinical models recapitulating alcohol-induced, virus-related and NASH-HCC as well as molecular subclasses G1–6. By matching chromosomal aberrations of mouse and human tumors, it is possible to construct an algorithm to measure the concordance (*P* value) of a model and a specific patient subgroup. As previously reported, synteny studies efficiently compare homologue mouse and human chromosomal aberrations (37). Sequencing of tumor suppressors and oncogenes might also be helpful to identify molecular markers, though mutational profiles of murine liver tumors largely differ from human HCC. For example, we found *BRAF* and *HRAS* mutations (rare in humans) as was reported in previous studies (23, 35). The absence of *TP53* mutations in murine tumors is in line with earlier findings (15) and stands in contrast to human HCC. *CTNNB1* mutations, found in 27% of human HCC regardless of their etiology (38), were present only in two models (c-Myc and Mcl-1$^{\Delta hep}$). Recently, a study with design similar to ours was performed by Dow and colleagues based on genomic and transcriptomic profiles in mouse versus human tumor tissues (39). The authors claim that distinct mouse models reflect aspects of

Published OnlineFirst April 9, 2019; DOI: 10.1158/1541-7786.MCR-18-1045

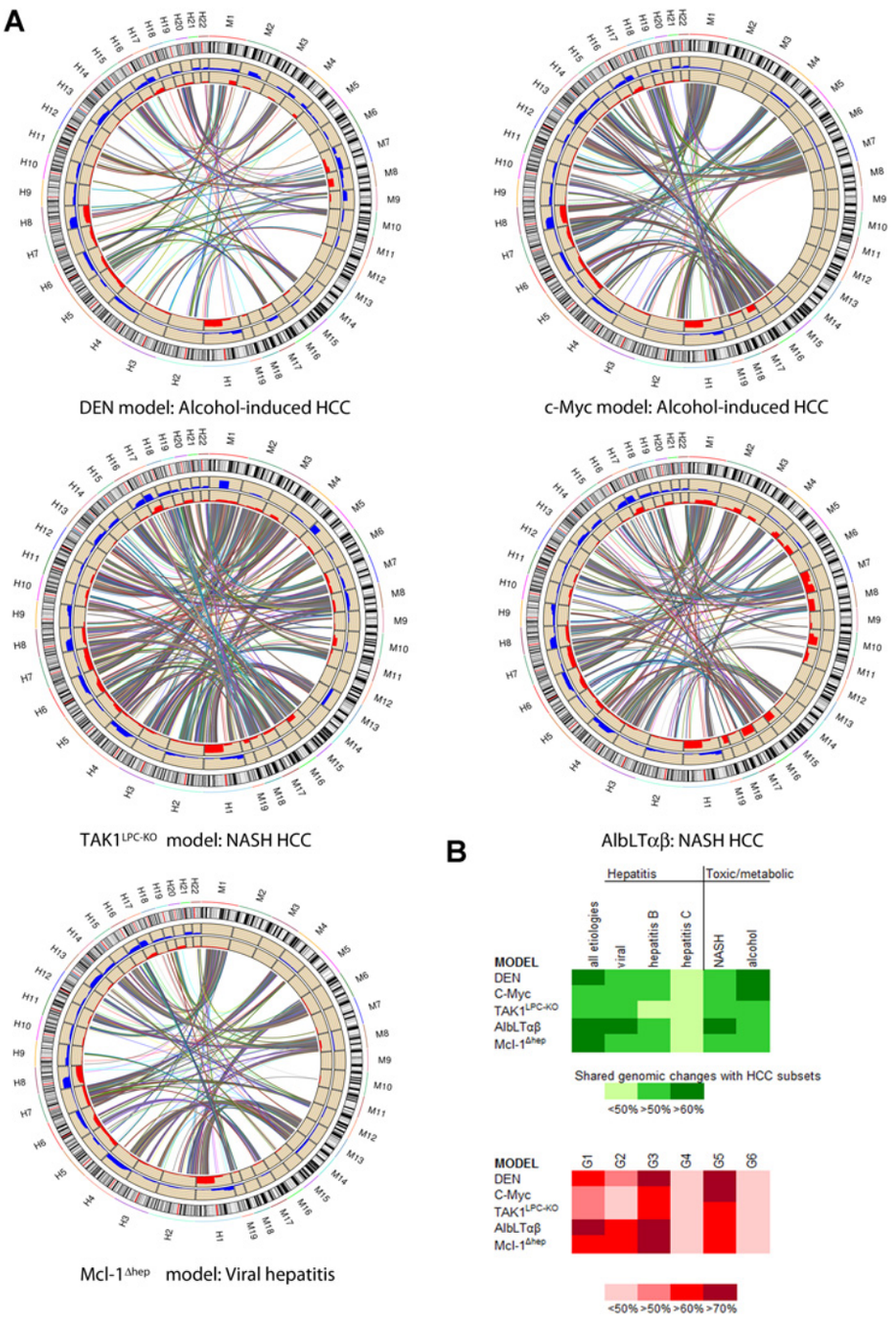

Figure 2
Etiology-dependent subtype approach of matching murine and human liver tumors based on CGH. **A,** Circular plots of synteny analysis comparing chromosomal aberrations of murine (M1–19) and human (H1–22) liver tumors. Inner circle (red) shows losses; outer circle (blue) shows gains. The closest match for the etiology-dependent patient subset (bottom line) and each mouse model is represented by the combined matches of gains and losses. **B,** Combined matches (gains and losses) of each model compared with the TCGA HCC cohort (LIHC; http://cancergenome.nih.gov/): etiology-oriented patient subsets (green, top heat map) as well as molecular subclasses (Boyault et al. 2007) G1–6 (red, bottom heat map). Colors indicate concordance as follows: light green/red (<50%), green/red (>50%), and dark green/red (>60% or >70%). "All etiologies" comprises matching of genomic changes accounting for the unstratified TCGA set of human HCC. Numbers increase with specificity of genomic aberrations.

low-grade human tumors, whereas, e.g., DEN tumors carry a high mutational burden similar to poorly differentiated tumors. Going beyond the molecular level, we have aimed to perform a comprehensive approach integrating morphologic, IHC, and CGH analysis to assess human–mouse similarities.

The correlation we observed between histopathologic characteristics and CGH results supports the etiology-oriented subtyping of HCC mouse models accounting for heterogeneity of disease (33, 40, 41). A recent study by Calderaro and colleagues reported the relationship between heterogeneous histologic subtypes and associated oncogenic pathways in HCC (42). As was demonstrated in our analysis, intracellular hyaline bodies are abundant in DEN-induced tumors that most closely matched alcohol-induced HCC. The cellular inclusions are reminiscent of Mallory–Denk bodies, typical for human alcoholic steatohepatitis. The rounder hyaline bodies and irregular, keratin 8 containing Mallory bodies (43) coexisted in a study on 174 human HCC in 7.5% of cases (44). A crucial finding is also the presence of steatosis, indicative of metabolic deregulation (9) characteristic for NASH patients.

Published OnlineFirst April 9, 2019; DOI: 10.1158/1541-7786.MCR-18-1045

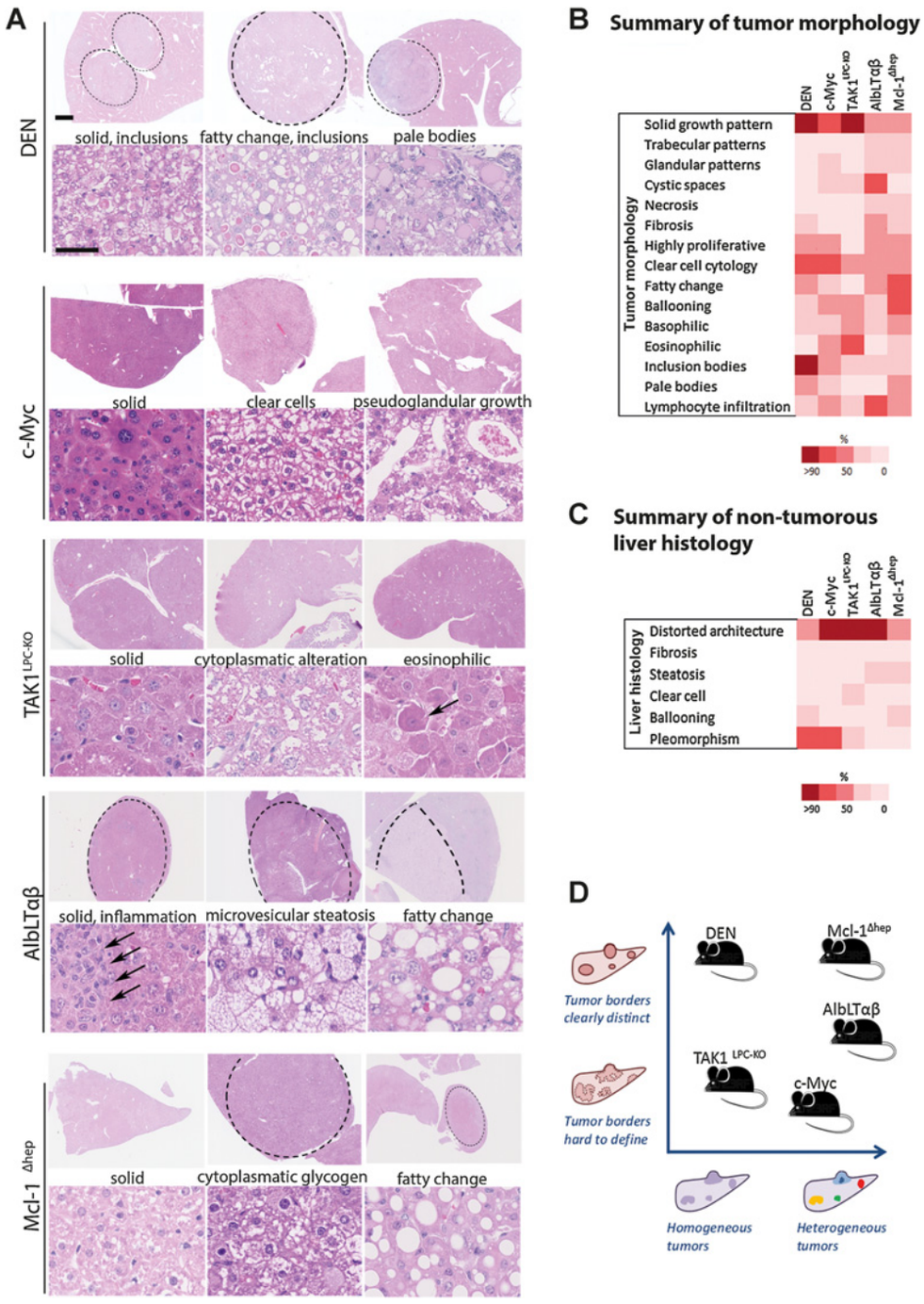

Figure 3

Growth patterns, cytological features and immune infiltration of murine liver tumors. **A,** Histologic patterns ranging in murine tumors (TAK1^{LPC-KO} and DEN, c-Myc, AlbLTαβ, and Mcl-1$^{\Delta hep}$), involving solid growth, clear cell cytology, and fatty change. Scale bars (overview) indicate 1 mm (overviews) and 50 μm (30 × magnification). **B,** Summarized features of tumor architecture, growth patterns, and cytological features of murine liver tumors and (**C**) surrounding liver tissue. Heat map indicates a semiquantitative analysis of respective histologic features in the number of murine tumors, faint red: not present-up to dark red: feature present in all/almost all tumors. **D,** Schematic illustration of tumor heterogeneity and tumor borders in different murine models.

NASH/cryptogenic HCC were best recapitulated by tumors of the AlbLTαβ and TAK1^{LPC-KO} model. Particularly the AlbLTαβ model showed features diagnostic for NASH such as steatosis and inflammatory infiltration(45, 46) criteria for diagnosing NAFLD/NASH. Even though the model was originally developed to mimic human chronic viral hepatitis (10), the

Published OnlineFirst April 9, 2019; DOI: 10.1158/1541-7786.MCR-18-1045

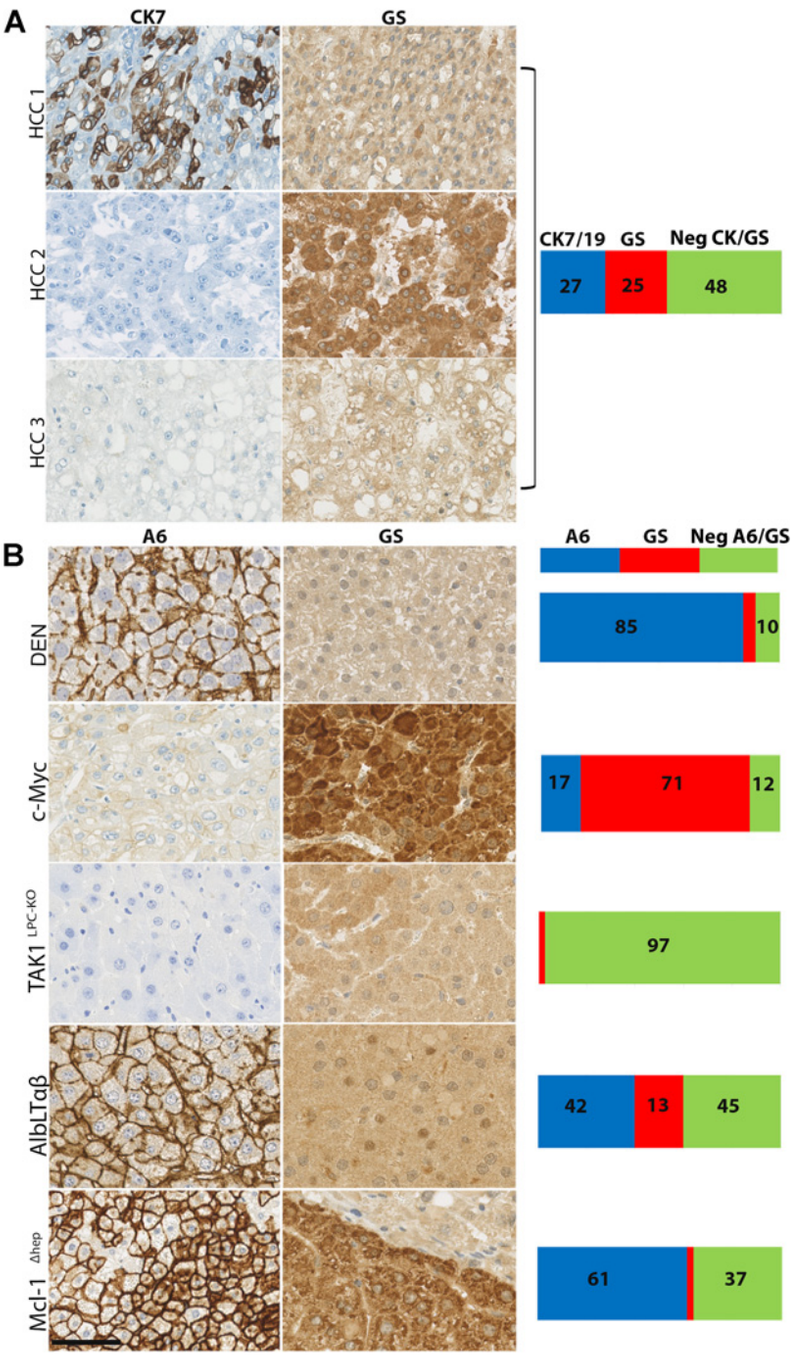

Figure 4

IHC profiles of human versus murine liver tumors. **A,** IHC profiles of $n = 61$ HCC patients depicted by stacked bar plots. Profiles were assessed by duplicate TMA spots for glutamine synthetase (GS indicating β-catenin activation) and CK7/CK19 stainings indicating stem-like phenotypes. **−/−** indicates that none of the two marker was positive. Numbers declare percentages of tumors showing positivity for the respective marker. Pictures show representative stainings of three HCCs: HCC1 $CK7^+$ and GS^-, associated with alcohol abuse. HCC2 represents GS^+ and $CK7^-$ group, associated with hepatitis C. HCC3 represents the double-negative group, the patient had none of the known risk factors (cryptogenic). Scale bar, 50 μm in 30 × magnification. **B,** IHC profiles illustrated by stacked bar plots of murine liver lesions classified as "tumors," grouped by model. A6 is considered to correspond to CK7 in humans. GS: glutamine synthetase. Neg A6/GS was used if none of the two markers was positive. Numbers declare percentages of tumors showing positivity for the respective marker. Subnodules, i.e., tumor regions with different immunophenotypes within larger lesions, were included in the analysis. Side-by-side pictures do represent examples (not necessarily same tumor area).

current analysis found more similarities with NASH-induced HCC. Fibrosis, an important feature of human chronic liver disease, was rare in murine models, as has been documented before (47).

One of the key observations of this study is that inter- and intratumor heterogeneity is present in varying degrees in HCC mouse models, which could be considered as an indicator of the appropriateness of murine models. Although human HCC typically show inter- and intratumor heterogeneity (33), this feature is recapitulated only by particular liver cancer models (Mcl-$1^{\Delta hep}$, c-Myc, and AlbLTαβ). Taking into account inter- and intratumor heterogeneity in preclinical models is crucial for many solid cancer models, especially for testing systemic treatments in advanced disease. Suitable preclinical animal models recapitulating diverse histopathology, IHC profiles, and associated oncogenic pathways of human HCC subtypes can be expected to better recapitulate reponsiveness to treatment.

Published OnlineFirst April 9, 2019; DOI: 10.1158/1541-7786.MCR-18-1045

Table 3. Summary of mouse model subtyping results in comparison with respective HCC patient subsets (TCGA)

Model	Etiology-based CGH/synteny	G1–6 groups CGH/synteny	Histologic features	IHC profiles	Immune infiltration	Inter-/intratumor heterogeneity
DEN	Alcohol-induced	G3/G5	Inclusion bodies, fibrosis (in tumors), steatosis	Only stem/biliary-like phenotypes	Scarce	No/No
c-Myc	Alcohol-induced	G5	Pleomorphism, clear cell foci	WNT activation	Moderate	Yes/No
AlbLTαβ	NASH-associated	G3	Fatty change, steatosis, massive lymphocyte infiltration	Stem/biliary-like >WNT activation	Severe	Yes/Yes
TAK1^{LPC-KO}	NASH-associated	G3/G5	Signs of liver injury (eosinophilic change)	**No** WNT activation **No** Stem/biliary-like	Scarce	No/No
Mcl-1$^{\Delta hep}$	Viral hepatitis	G3	Highly proliferative, steatosis, fatty change, lymphocyte infiltration	Stem/biliary-like>>WNT activation	Moderate	Yes/Yes

A limitation of our study is that intratumor heterogeneity was analyzed only on the level of morphology and IHC. In line with earlier findings, phenotype–genotype correlation studies have shown that genetic heterogeneity frequently goes along with morphologic and immune-phenotypic heterogeneity (33). Because we could not find morphologic and/or immune-phenotypical intratumor heterogeneity except for nodule-in-nodule growth in one model (Mcl-1$^{\Delta hep}$), we did not follow up on microdissection of the lesions. Another limitation of our study regards imaging and treatment responses in preclinical models, which were performed in a study by Gross and colleagues (12). This study compared the DEN model with the allograft model McA looking at tumor imaging in conjunction with histopathology, CGH, and treatment response.

Regarding the recent interest in the immune microenviroment (48, 49) with focus on T cells in NASH (37, 50), mainly the AlbLTαβ model seems to have the potential for consecutive subtyping of lymphocytes and PD-L1 expression analysis. A response rate of 20% for PD-1 (anti-programmed cell death-1 antibody) monotherapy in phase I/II trials has been attributed to the refractory immune-suppressive status in liver cancer patients (51), which needs further investigation.

In summary, contemporary preclinical models may be assigned to etiology-dependent patient groups and should account for inter- and intratumor heterogeneity. This holds implications for the preclinical testing of targeted treatments and could improve patient management.

Disclosure of Potential Conflicts of Interest

No potential conflicts of interest were disclosed.

Authors' Contributions

Conception and design: J. Friemel, L. Frick, M. Heikenwalder, A. Weber
Development of methodology: L. Frick, A. Weber
Acquisition of data (provided animals, acquired and managed patients, provided facilities, etc.): J. Friemel, L. Frick, K. Unger, M. Egger, R. Parrotta, A. Adili, T. Luedde, M. Heikenwalder, A. Weber
Analysis and interpretation of data (e.g., statistical analysis, biostatistics, computational analysis): J. Friemel, L. Frick, K. Unger, R. Parrotta, Y.T. Böge, M. Karin, M. Heikenwalder, A. Weber
Writing, review, and/or revision of the manuscript: J. Friemel, L. Frick, M. Karin, T. Luedde, M. Heikenwalder, A. Weber
Administrative, technical, or material support (i.e., reporting or organizing data, constructing databases): J. Friemel, A. Weber
Study supervision: M. Heikenwalder, A. Weber
Other (ran the experiment (aCGH array) and analyzed the acquired data): A. Adili

Acknowledgments

A. Weber was supported by a grant from the Swiss Cancer League (Oncosuisse). M. Heikenwalder was supported by an ERC Consolidator grant (HepatoMetaboPath); the DKFZ MOST program, the SFB 209, and the HepCAR 2020. T. Luedde was supported by a Mildred-Scheel Endowed Professorship from the German Cancer Aid (Deutsche Krebshilfe) and the German Research Foundation (DFG) (LU 1360/3-1 and SFB-TRR57/P06). The results published here are, in whole or part, based upon data generated by the TCGA Research Network: http://cancergenome.nih.gov/.

The costs of publication of this article were defrayed in part by the payment of page charges. This article must therefore be hereby marked *advertisement* in accordance with 18 U.S.C. Section 1734 solely to indicate this fact.

Received September 26, 2018; revised February 18, 2019; accepted April 3, 2019; published first April 9, 2019.

References

1. El-Serag HB, Kanwal F.Epidemiology of hepatocellular carcinoma in the United States: where are we? Where do we go? Hepatology 2014;60: 1767–75.
2. Torre LA, Bray F, Siegel RL, Ferlay J, Lortet-Tieulent J, Jemal A.Global cancer statistics, 2012. CA Cancer J Clin 2015;65:87–108.
3. Mittal S, El-Serag HB.Epidemiology of hepatocellular carcinoma: consider the population. J Clin Gastroenterol 2013;47Suppl:S2–6.
4. Michelotti GA, Machado MV, Diehl AM. NAFLD, NASH and liver cancer. Nat Rev Gastroenterol Hepatol 2013;10:656–65.
5. Ascha MS, Hanouneh IA, Lopez R, Tamimi TA, Feldstein AF, Zein NN. The incidence and risk factors of hepatocellular carcinoma in patients with nonalcoholic steatohepatitis. Hepatology 2010;51:1972–8.
6. Gengenbacher N, Singhal M, Augustin HG. Preclinical mouse solid tumour models: status quo, challenges and perspectives. Nat Rev Cancer 2017;17: 751–65.
7. Maeda S, Kamata H, Luo JL, Leffert H, Karin M. IKKbeta couples hepatocyte death to cytokine-driven compensatory proliferation that promotes chemical hepatocarcinogenesis. Cell 2005;121:977–90.
8. Vick B, Weber A, Urbanik T, Maass T, Teufel A, Krammer PH, et al. Knockout of myeloid cell leukemia-1 induces liver damage and increases apoptosis susceptibility of murine hepatocytes. Hepatology 2009;49:627–36.
9. Thoolen B, Maronpot RR, Harada T, Nyska A, Rousseaux C, Nolte T, et al. Proliferative and nonproliferative lesions of the rat and mouse hepatobiliary system. Toxicol Pathol 2010;38:5S–81S.
10. Haybaeck J, Zeller N, Wolf MJ, Weber A, Wagner U, Kurrer MO, et al. A lymphotoxin-driven pathway to hepatocellular carcinoma. Cancer Cell. 2009;16:295–308.
11. Weber A, Boger R, Vick B, Urbanik T, Haybaeck J, Zoller S, et al. Hepatocyte-specific deletion of the antiapoptotic protein myeloid cell leukemia-1 triggers proliferation and hepatocarcinogenesis in mice. Hepatology 2010;51:1226–36.
12. Gross C, Steiger K, Sayyed S, Heid I, Feuchtinger A, Walch A, et al. Model matters: differences in orthotopic rat hepatocellular carcinoma physiology determine therapy response to sorafenib. Clin Cancer Res 2015;21: 4440–50.

13. de La Coste A, Romagnolo B, Billuart P, Renard CA, Buendia MA, Soubrane O, et al. Somatic mutations of the beta-catenin gene are frequent in mouse and human hepatocellular carcinomas. Proc Natl Acad Sci U S A 1998;95: 8847–51.
14. Devereux TR, Anna CH, Foley JF, White CM, Sills RC, Barrett JC. Mutation of beta-catenin is an early event in chemically induced mouse hepatocellular carcinogenesis. Oncogene 1999;18:4726–33.
15. Kress S, Konig J, Schweizer J, Lohrke H, Bauer-Hofmann R, Schwarz M. p53 mutations are absent from carcinogen-induced mouse liver tumors but occur in cell lines established from these tumors. Mol Carcinog 1992;6: 148–58.
16. Thorgeirsson SS, Santoni-Rugiu E. Transgenic mouse models in carcinogenesis: interaction of c-myc with transforming growth factor alpha and hepatocyte growth factor in hepatocarcinogenesis. Br J Clin Pharmacol 1996;42:43–52.
17. Bettermann K, Vucur M, Haybaeck J, Koppe C, Janssen J, Heymann F, et al. TAK1 suppresses a NEMO-dependent but NF-kappaB-independent pathway to liver cancer. Cancer Cell 2010;17:481–96.
18. Boege Y, Malehmir M, Healy ME, Bettermann K, Lorentzen A, Vucur M, et al. A dual role of caspase-8 in triggering and sensing proliferation-associated DNA damage, a key determinant of liver cancer development. Cancer Cell 2017;32:342–59e10.
19. Inokuchi-Shimizu S, Park EJ, Roh YS, Yang L, Zhang B, Song J, et al. TAK1-mediated autophagy and fatty acid oxidation prevent hepatosteatosis and tumorigenesis. J Clin Invest 2014;124:3566–78.
20. Vucur M, Reisinger F, Gautheron J, Janssen J, Roderburg C, Cardenas DV, et al. RIP3 inhibits inflammatory hepatocarcinogenesis but promotes cholestasis by controlling caspase-8- and JNK-dependent compensatory cell proliferation. Cell Rep 2013;4:776–90.
21. Huang H, Ushijima T, Nagao M, Sugimura T, Ohgaki H. Beta-catenin mutations in liver tumors induced by 2-amino-3,4-dimethylimidazo[4,5-f]quinoline in CDF1 mice. Cancer Lett 2003;198:29–35.
22. Calvert RJ, Tashiro Y, Buzard GS, Diwan BA, Weghorst CM. Lack of p53 point mutations in chemically induced mouse hepatoblastomas: an end-stage, highly malignant hepatocellular tumor. Cancer Lett 1995;95: 175–80.
23. Jaworski M, Buchmann A, Bauer P, Riess O, Schwarz M. B-raf and Ha-ras mutations in chemically induced mouse liver tumors. Oncogene 2005;24: 1290–5.
24. Greenberg RA, Allsopp RC, Chin L, Morin GB, DePinho RA. Expression of mouse telomerase reverse transcriptase during development, differentiation and proliferation. Oncogene 1998;16:1723–30.
25. Pericuesta E, Ramirez MA, Villa-Diaz A, Relano-Gines A, Torres JM, Nieto M, et al. The proximal promoter region of mTert is sufficient to regulate telomerase activity in ES cells and transgenic animals. Reprod Biol Endocrinol 2006;4:5.
26. Mu X, Espanol-Suner R, Mederacke I, Affo S, Manco R, Sempoux C, et al. Hepatocellular carcinoma originates from hepatocytes and not from the progenitor/biliary compartment. J Clin Invest 2015;125:3891–903.
27. Wienberg J. The evolution of eutherian chromosomes. Curr Opin Genet Dev 2004;14:657–66.
28. Caldwell SH, Oelsner DH, Iezzoni JC, Hespenheide EE, Battle EH, Driscoll CJ. Cryptogenic cirrhosis: clinical characterization and risk factors for underlying disease. Hepatology 1999;29:664–9.
29. Ertle J, Dechene A, Sowa JP, Penndorf V, Herzer K, Kaiser G, et al. Non-alcoholic fatty liver disease progresses to hepatocellular carcinoma in the absence of apparent cirrhosis. Int J Cancer 2011;128: 2436–43.
30. Torres DM, Harrison SA. Nonalcoholic steatohepatitis and noncirrhotic hepatocellular carcinoma: fertile soil. Semin Liver Dis 2012;32: 30–8.
31. Boyault S, Rickman DS, de Reynies A, Balabaud C, Rebouissou S, Jeannot E, et al. Transcriptome classification of HCC is related to gene alterations and to new therapeutic targets. Hepatology 2007;45:42–52.
32. Hoshida Y. Nearest template prediction: a single-sample-based flexible class prediction with confidence assessment. PLoS One 2010;5:e15543.
33. Friemel J, Rechsteiner M, Frick L, Bohm F, Struckmann K, Egger M, et al. Intratumor heterogeneity in hepatocellular carcinoma. Clin Cancer Res 2015;21:1951–61.
34. Malz M, Weber A, Singer S, Riehmer V, Bissinger M, Riener MO, et al. Overexpression of far upstream element binding proteins: a mechanism regulating proliferation and migration in liver cancer cells. Hepatology 2009;50:1130–9.
35. He G, Dhar D, Nakagawa H, Font-Burgada J, Ogata H, Jiang Y, et al. Identification of liver cancer progenitors whose malignant progression depends on autocrine IL-6 signaling. Cell 2013;155:384–96.
36. Hale G, Liu X, Hu J, Xu Z, Che L, Solomon D, et al. Correlation of exon 3 beta-catenin mutations with glutamine synthetase staining patterns in hepatocellular adenoma and hepatocellular carcinoma. Mod Pathol 2016;29:1370–80.
37. Wolf MJ, Adili A, Piotrowitz K, Abdullah Z, Boege Y, Stemmer K, et al. Metabolic activation of intrahepatic CD8+ T cells and NKT cells causes nonalcoholic steatohepatitis and liver cancer via cross-talk with hepatocytes. Cancer Cell 2014;26:549–64.
38. Cancer Genome Atlas Research Network. Comprehensive and integrative genomic characterization of hepatocellular carcinoma. Cell 2017;169: 1327–41.
39. Dow M, Pyke RM, Tsui BY, Alexandrov LB, Nakagawa H, Taniguchi K, et al. Integrative genomic analysis of mouse and human hepatocellular carcinoma. Proc Natl Acad Sci U S A 2018;115:E9879–88.
40. Friemel J, Rechsteiner M, Bawohl M, Frick L, Mullhaupt B, Lesurtel M, et al. Liver cancer with concomitant TP53 and CTNNB1 mutations: a case report. BMC Clin Pathol 2016;16:7.
41. Zhai W, Lim TK, Zhang T, Phang ST, Tiang Z, Guan P, et al. The spatial organization of intra-tumour heterogeneity and evolutionary trajectories of metastases in hepatocellular carcinoma. Nat Commun 2017;8:4565.
42. Calderaro J, Couchy G, Imbeaud S, Amaddeo G, Letouze E, Blanc JF, et al. Histological subtypes of hepatocellular carcinoma are related to gene mutations and molecular tumour classification. J Hepatol 2017;67: 727–38.
43. Mahajan V, Klingstedt T, Simon R, Nilsson KP, Thueringer A, Kashofer K, et al. Cross beta-sheet conformation of keratin 8 is a specific feature of Mallory-Denk bodies compared with other hepatocyte inclusions. Gastroenterology 2011;141:1080–90.
44. Denk H, Stumptner C, Fuchsbichler A, Muller T, Farr G, Muller W, et al. Are the Mallory bodies and intracellular hyaline bodies in neoplastic and non-neoplastic hepatocytes related? J Pathol 2006;208:653–61.
45. Brunt EM, Kleiner DE, Wilson LA, Belt P, Neuschwander-Tetri BA, NASH Clinical Research Network (CRN). Nonalcoholic fatty liver disease (NAFLD) activity score and the histopathologic diagnosis in NAFLD: distinct clinicopathologic meanings. Hepatology 2011;53:810–20.
46. Caldwell SH, Lee VD, Kleiner DE, Al-Osaimi AM, Argo CK, Northup PG, et al. NASH and cryptogenic cirrhosis: a histological analysis. Ann Hepatol 2009;8:346–52.
47. Reiberger T, Chen Y, Ramjiawan RR, Hato T, Fan C, Samuel R, et al. An orthotopic mouse model of hepatocellular carcinoma with underlying liver cirrhosis. Nat Protoc 2015;10:1264–74.
48. Heikenwalder M, Pikarsky E. Learning the roles of the hepatic adaptive immune system in hepatocellular carcinoma—nature's guide for successful cancer immunotherapy. Semin Liver Dis 2017;37:210–8.
49. Pikarsky E, Heikenwalder M. Focal and local: ectopic lymphoid structures and aggregates of myeloid and other immune cells in liver. Gastroenterology 2016;151:780–3.
50. Shalapour S, Lin XJ, Bastian IN, Brain J, Burt AD, Aksenov AA, et al. Inflammation-induced IgA+ cells dismantle anti-liver cancer immunity. Nature 2017;551:340–5.
51. Nishida N, Kudo M. Immune checkpoint blockade for the treatment of human hepatocellular carcinoma. Hepatol Res 2018;48:622–34.

Published OnlineFirst April 9, 2019; DOI: 10.1158/1541-7786.MCR-18-1045

American Association for Cancer Research

Molecular Cancer Research

Characterization of HCC Mouse Models: Towards an Etiology-Oriented Subtyping Approach

Juliane Friemel, Lukas Frick, Kristian Unger, et al.

Mol Cancer Res 2019;17:1493-1502. Published OnlineFirst April 9, 2019.